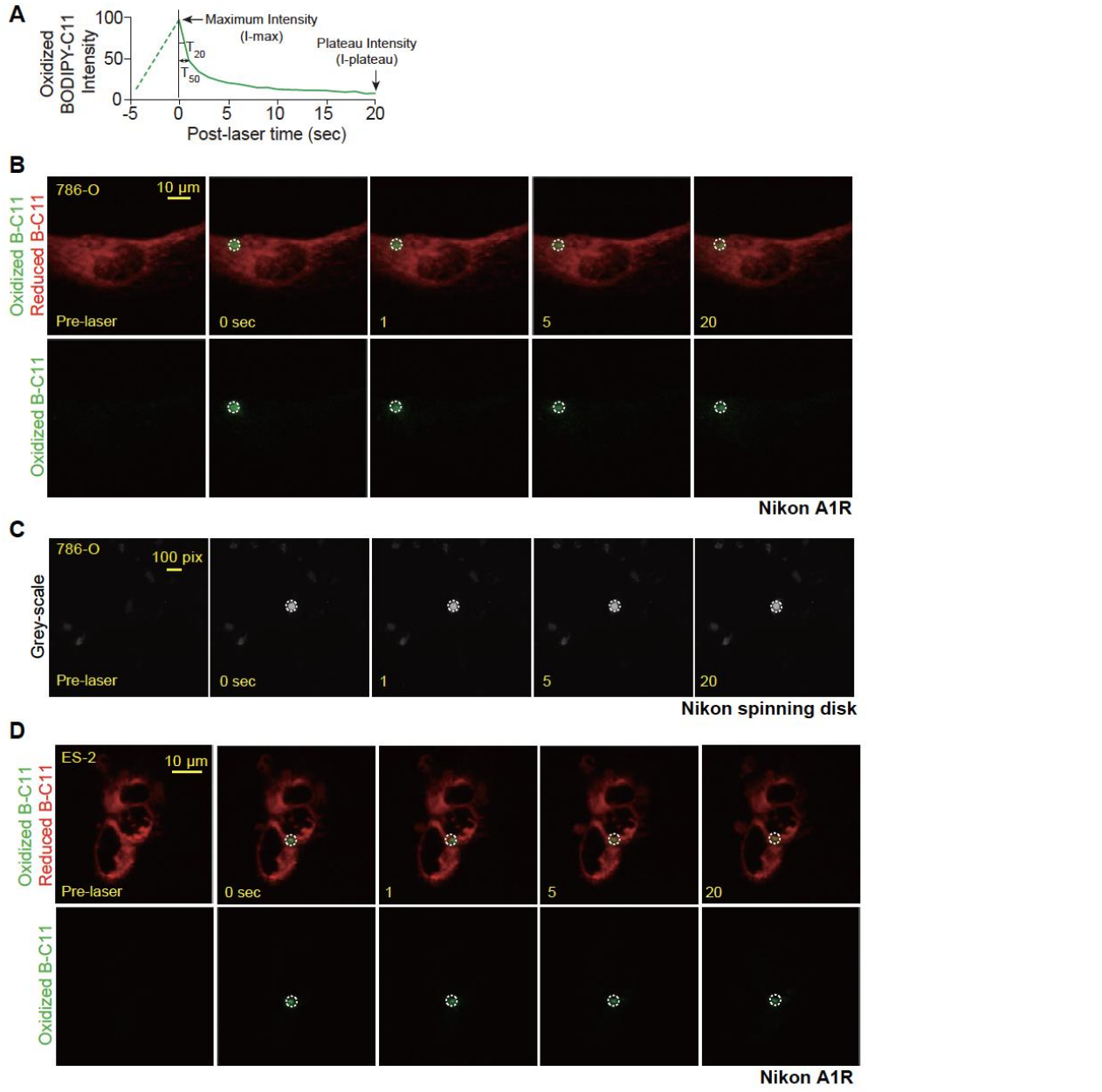
A
Oxidized BODIPY-C11 Intensity
100
50
0
-5
0
5
10
15
20
Post-laser time (sec)
Maximum Intensity (I-max)
Plateau Intensity (I-plateau)
T20
T50
B
786-O
10 μm
Oxidized B-C11
Reduced B-C11
Pre-laser
0 sec
1
5
20
Oxidized B-C11
Nikon A1R
C
786-O
100 pix
Grey-scale
Pre-laser
0 sec
1
5
20
Nikon spinning disk
D
ES-2
10 μm
Oxidized B-C11
Reduced B-C11
Pre-laser
0 sec
1
5
20
Oxidized B-C11
Nikon A1R
E
Before PALP
Post PALP
NRK
Oxidized B-C11
Reduced B-C11
Oxidized B-C11
Reduced B-C11
0.1s
7.19s
13.62s
24.38s
10 μm
F
Before PALP
Post PALP
L929
Oxidized B-C11
Reduced B-C11
Oxidized B-C11
Reduced B-C11
0.1s
7.19s
13.62s
24.38s
10 μm

Supplementary Figure 1. Targeted laser pulses induce localized lipid peroxidation in live cancer cells (related to Figure 1). Green, oxidized BODIPY-C11 signal; red, reduced BODIPY-C11 signal.

A. Schematic diagram showing the parameters used to describe the dynamics of lipid peroxidation signal in a representative PALPv1 experiment. All oxidized BODIPY-C11 signals are normalized by deducing the pre-laser intensity from the detected signals. I-max, normalized maximal intensity, T_{20}, time (sec) it takes to reach 20% reduction from I-max signal. T_{50}, time (sec) it takes to reach 50% reduction from I-max signal. I-plateau, normalized signal intensity when the oxBODIPY-C11 signal largely plateaued.

B. Representative fluorescent images showing the reduced and oxidized BODIPY-C11 signal before and after the application of 405 nm laser pulses in 786-O cells acquired on a Nikon A1R HD25 confocal microscope. Scale bar indicates 10 µm.

C. Representative fluorescent images showing the oxidized BODIPY-C11 signal before and after the application of 405 nm laser pulses PALP signals in 786-O cells acquired on a Nikon spinning disk confocal CSU-W1 system. Scale bar indicates 100 pix.

D. Representative fluorescent images showing the reduced and oxidized BODIPY-C11 signal before and after the application of 405 nm laser pulses in ES-2 cells acquired on a Nikon A1R HD25 confocal microscope. Scale bar indicates 10 µm.

E. Representative fluorescent images showing the reduced and oxidized BODIPY-C11 signal before and after the application of 405 nm laser pulses in rat NRK cells acquired on a Nikon A1 N-SIM STORM confocal microscope. This experiment was performed twice.

F. Representative fluorescent images showing the reduced and oxidized BODIPY-C11 signal before and after the application of 405 nm laser pulses in mouse L929 cells acquired on a Nikon A1 N-SIM STORM confocal microscope. This experiment was performed twice.

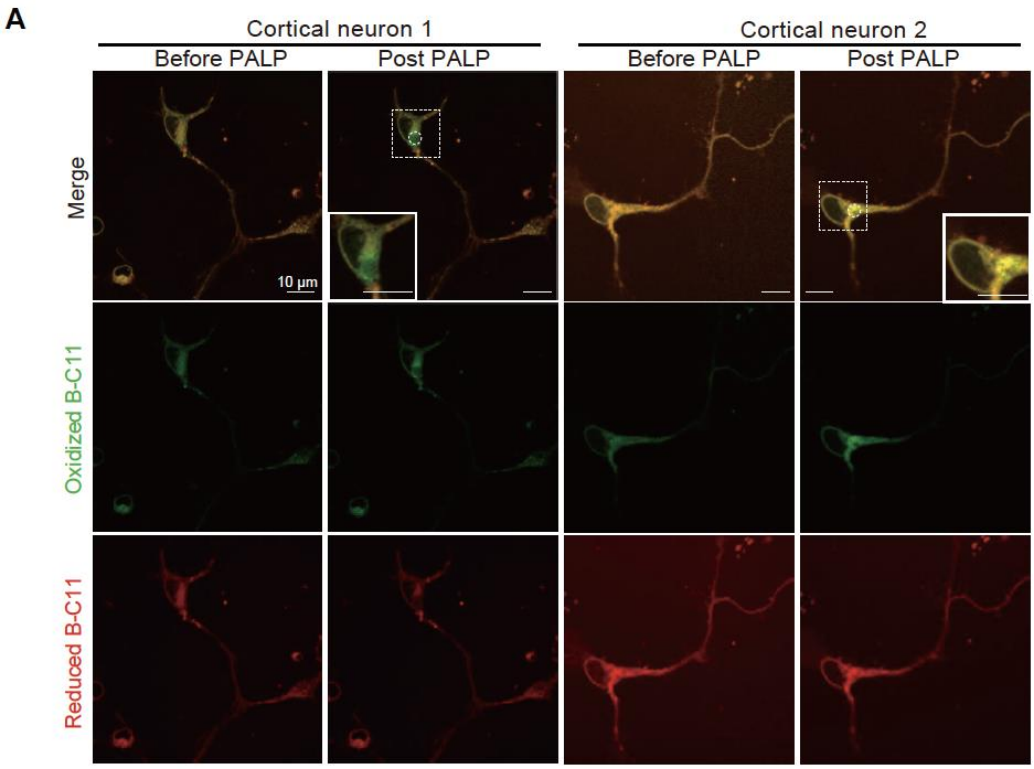
A
Cortical neuron 1
Cortical neuron 2
Before PALP
Post PALP
Before PALP
Post PALP
Merge
10 μm
Oxidized B-C11
Reduced B-C11

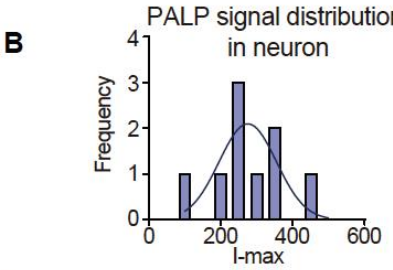
B
PALP signal distribution
in neuron
Frequency
0
1
2
3
4
0
200
400
600
l-max

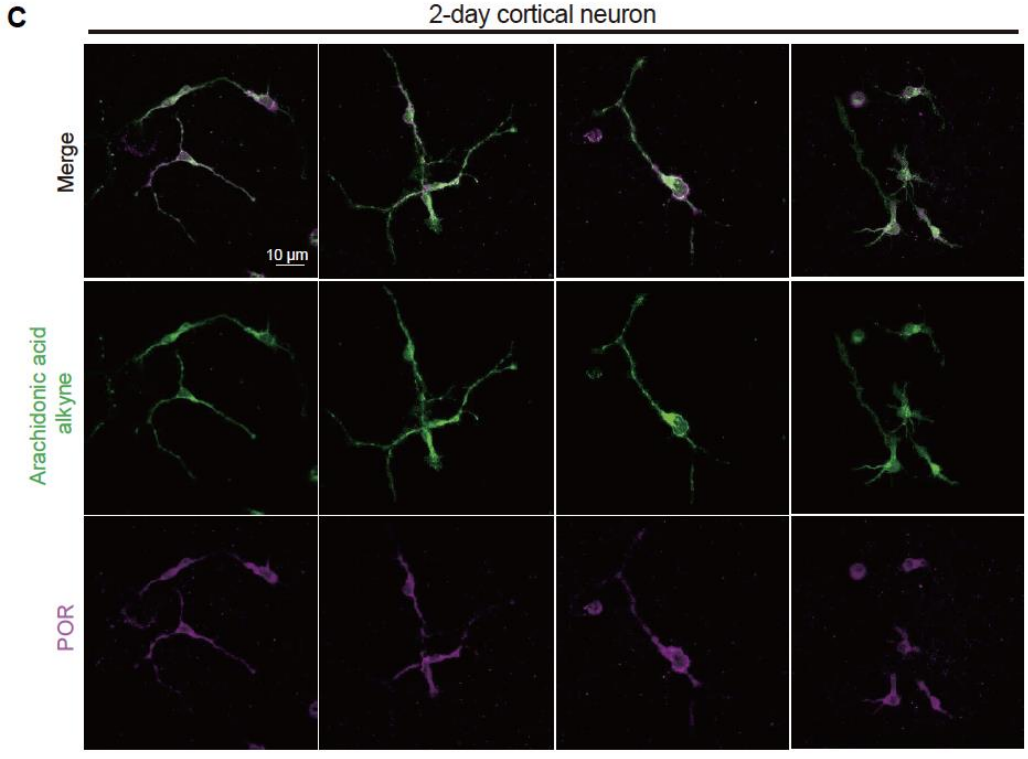
C
2-day cortical neuron
Merge
10 μm
Arachidonic acid
alkyne
POR

Supplementary Figure 2. Targeted laser pulses induce localized lipid peroxidation in primary mouse cortical neurons (related to Figure 1).

A. Representative fluorescent images showing the reduced and oxidized BODIPY-C11 signal before and after the application of 405 nm laser pulses in primary mouse neurons in culture (two additional cells from the same experiment as in **Figure 1C**). Green, oxidized BODIPY-C11 signal; red, reduced BODIPY-C11 signal. Scale bar indicates 10 µm.

B. Frequency distribution of the I-max signal intensity in 9 neurons analyzed by PALPv1. Gaussian nonlinear regression used to generate the fit curve.

C. Representative fluorescent images showing the localization of POR protein, used as an endoplasmic reticulum tracker, and exogenously added polyunsaturated fatty acid-alkyne in neurons. Cells were incubated with 5 µM arachidonic acid-alkyne for 18 hours prior to fixation. Green, arachidonic acid-alkyne signal; violet, POR signal. Scale bar indicates 10 µm. This experiment was performed once.

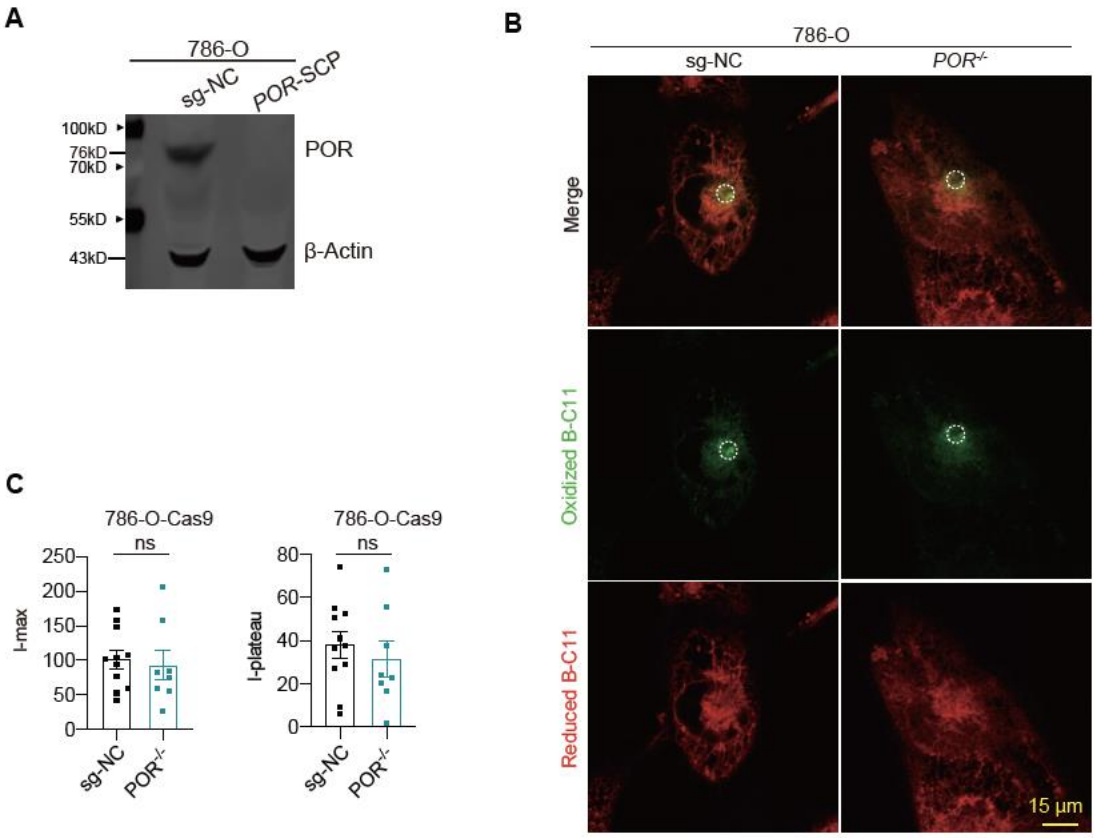

Supplementary Figure 3. PALPv1-induced fluorescence is likely independent of POR activity (related to Figure 2).

A. Immunoblot analysis of POR protein levels in sgNC-expressing or *POR* $^{-/-}$ 786-O cells. β-Actin was used as a loading control. This experiment was performed in duplicate.

B. Representative fluorescent images showing the I-max (0 sec) post the application of laser pulses to 786-O cells expressing sg-NC or *POR*$^{-/-}$ cells. Green, oxidized BODIPY-C11 signal; red, reduced BODIPY-C11 signal. This experiment was performed twice and 8-10 cells were analyzed for each group in each experiment.

C. Box-scatter plots showing the PALP parameters (I-max and I-plateau) of 786-O-Cas9 cells expressing sg-NC or a *POR*$^{-/-}$ 786-O single-cell clone. Dots and error bars, mean±s.d. Two-tailed, unpaired student's T-test. ns, not significant.

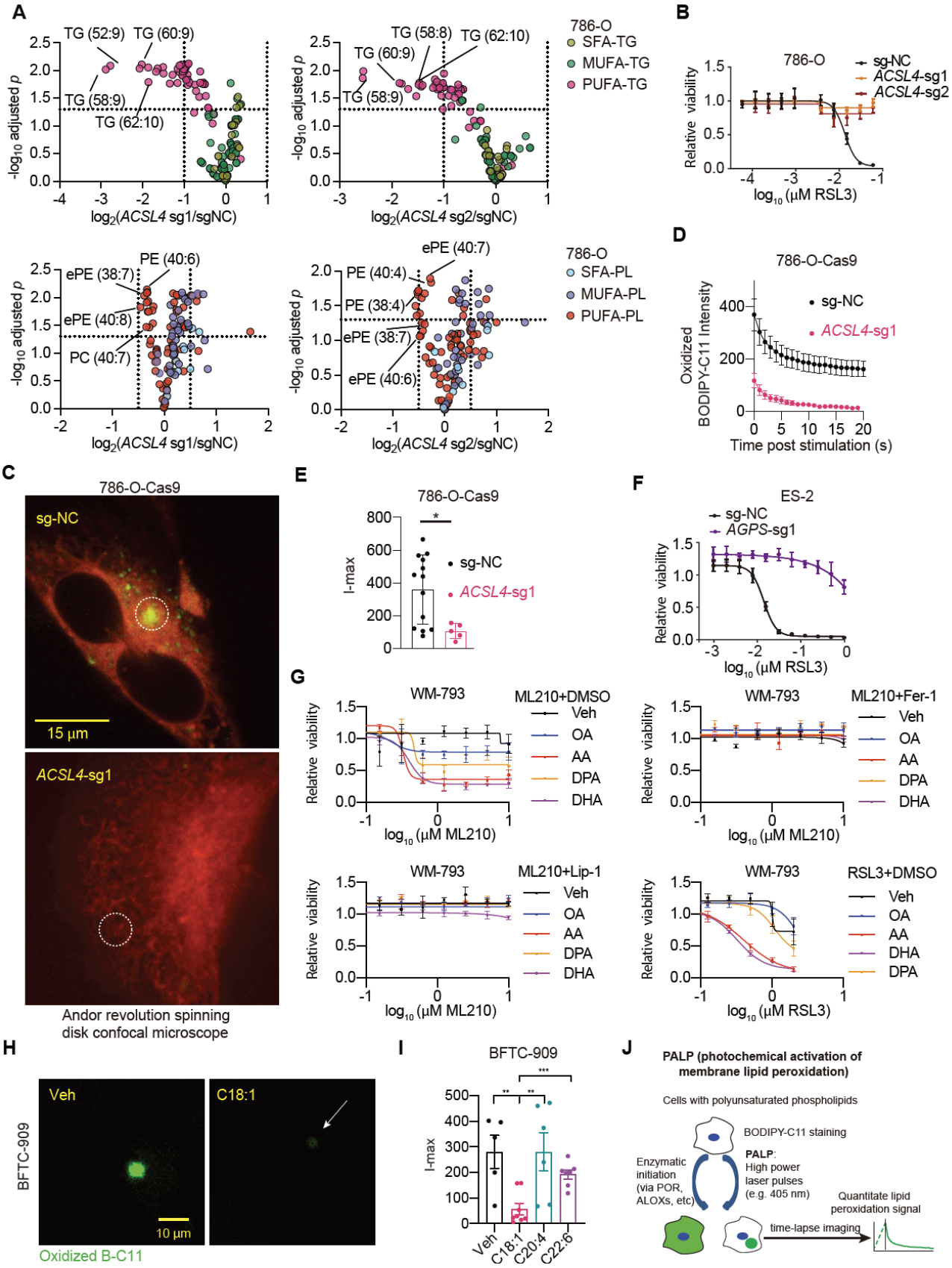
A
TG (52:9)
TG (60:9)
TG (58:9)
TG (62:10)
-log10 adjusted p
log2(ACSL4 sg1/sgNC)
TG (58:8)
TG (62:10)
log2(ACSL4 sg2/sgNC)
786-O
SFA-TG
MUFA-TG
PUFA-TG
PE (40:6)
ePE (38:7)
ePE (40:8)
PC (40:7)
ePE (40:7)
PE (40:4)
PE (38:4)
SFA-PL
MUFA-PL
PUFA-PL
B
786-O
sg-NC
ACSL4-sg1
ACSL4-sg2
Relative viability
log10 (μM RSL3)
D
786-O-Cas9
Oxidized BODIPY-C11 Intensity
Time post stimulation (s)
C
786-O-Cas9
sg-NC
15 μm
ACSL4-sg1
Andor revolution spinning disk confocal microscope
E
786-O-Cas9
I-max
F
ES-2
AGPS-sg1
G
WM-793
ML210+DMSO
ML210+Fer-1
ML210+Lip-1
RSL3+DMSO
Veh
OA
AA
DPA
DHA
log10 (μM ML210)
log10 (μM RSL3)
H
BFTC-909
Veh
C18:1
10 μm
Oxidized B-C11
I
BFTC-909
C18:1
C20:4
C22:6
J
PALP (photochemical activation of membrane lipid peroxidation)
Cells with polyunsaturated phospholipids
BODIPY-C11 staining
PALP:
High power laser pulses (e.g. 405 nm)
Enzymatic initiation (via POR, ALOXs, etc)
Quantitate lipid peroxidation signal
time-lapse imaging

Supplementary Figure 4. PALPv1-induced fluorescence is dependent on membrane polyunsaturated phospholipid levels (related to Figure 2).

A. Lipidomic analysis of 786-O cells expressing sg-NC or *ACSL4*-targeting sgRNAs. This experiment was performed twice. n=3 for each cell line condition. SFA, MUFA, PUFA, saturated, monounsaturated, or polyunsaturated fatty acids; TG, triacylglycerides; PL, phospholipids. PE, phosphatidylethanolamine; ePE, ether-linked PE; PC, phosphatidylcholine.

B. Viability curves of 786-O cells expressing sg-NC or sgRNAs targeting *ACSL4* treated with indicated concentrations of GPX4 inhibitor RSL3 for 48h. n=6; dots and error bars, mean±s.d. This experiment was repeated three times.

C. Representative fluorescent images showing the I-max (0 sec) post the application of laser pulses to 786-O cells expressing sg-NC or *ACSL4*-targeting sgRNA acquired on an Andor revolution spinning disk confocal microscope. Green, oxidized BODIPY-C11 signal; red, reduced BODIPY-C11 signal. Scale bar indicates 15 μm.

D. Quantifications of the PALP signal intensity from time-lapse imaging of 786-O cells expressing sg-NC or *ACSL4*-targeting sgRNA after laser activation. 5 cells were measured for each condition. Dots and error bars indicate mean±s.d..

E. Box-scatter plots showing the PALP I-max of 786-O cells expressing sg-NC or sgRNAs targeting *ACSL4*. Dots and error bars, mean±s.d. Two-tailed unpaired T-test, *, $p<0.05$.

F. Viability curves of ES-2 cells expressing sg-NC or sgRNAs targeting *AGPS* treated with indicated concentrations of GPX4 inhibitor RSL3 for 48h. n=6; error bar, mean±s.d. This experiment was repeated twice.

G. Viability curves for WM-793 cells treated with vehicle or indicated fatty acids, together with DMSO, Lip-1 or Fer-1 and indicated concentrations of ML210 or RSL3 for 48h. n=4; dots and error bars, mean±s.d. This experiment was performed once.

H. Box-scatter plots showing the I-max of PALP signals in BFTC-909 urothelial carcinoma cells treated with indicated free fatty acid. Two-tailed unpaired T-test, **, $p<0.01$, ***, $p<0.001$.

I. Representative fluorescent images showing the I-max (0 sec) post the application of laser pulses to BFTC-909 cells treated with vehicle or oleic acid (C18:1), arachidonic acid (C20:4) or DHA (C22:6). Green: oxidized BODIPY-C11 signal. Dots and error bars, mean±s.d. This experiment was performed twice.

J. Schematic diagram summarising the applications of PALP for detecting polyunsaturated phospholipid levels via photochemically-induced lipid peroxidation in live cells. PUFA, polyunsaturated fatty acyl-.

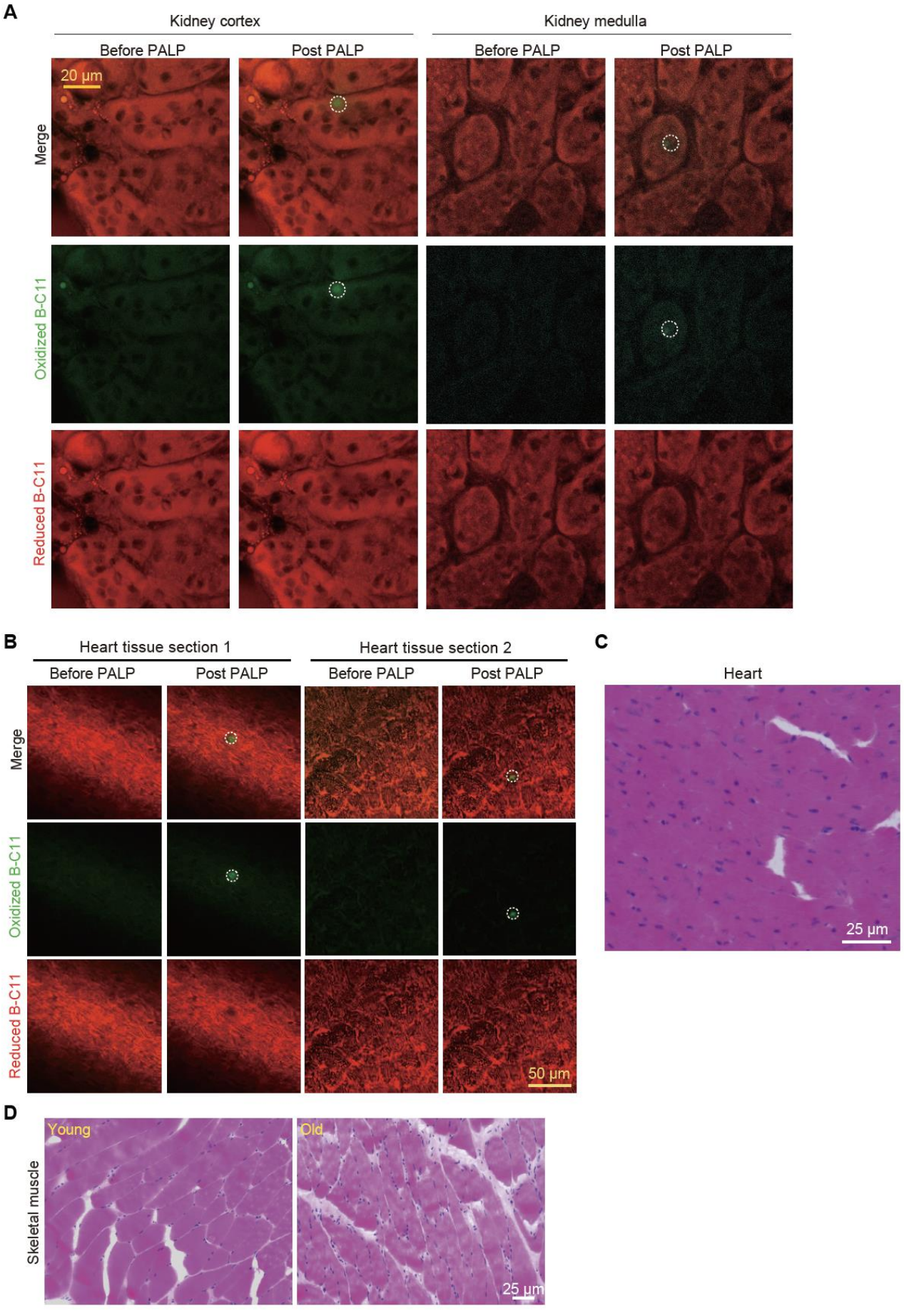
A
Kidney cortex
Kidney medulla
Before PALP
Post PALP
Before PALP
Post PALP
20 μm
Merge
Oxidized B-C11
Reduced B-C11
B
Heart tissue section 1
Heart tissue section 2
Before PALP
Post PALP
Before PALP
Post PALP
Merge
Oxidized B-C11
Reduced B-C11
50 μm
C
Heart
25 μm
D
Young
Old
Skeletal muscle
25 μm

Supplementary Figure 5. The PALPv1 technique can detect polyunsaturated phospholipids in mouse tissues *in situ* (related to Figure 5).

A. Representative fluorescent images showing PALP-induced fluorescence in cryo-sectioned mouse kidney tissue samples (two additional stimulated regions from the same experiment as **Figure 5C**).

B. Representative images showing PALP-induced fluorescence in cryo-sectioned mouse heart tissue samples (two additional regions from the same experiment as **Figure 5D**). Green, oxidized BODIPY-C11 signal; red, reduced BODIPY-C11 signal. Scale bar indicates 10 μm.

C. Histologic examination of longitudinal section of mouse heart using hematoxylin and eosin (H&E) staining. Original magnification X 400.

D. Histologic examination of longitudinal sections of mouse skeletal muscle using hematoxylin and eosin (H&E) staining from young and old mice. Original magnification X 200.

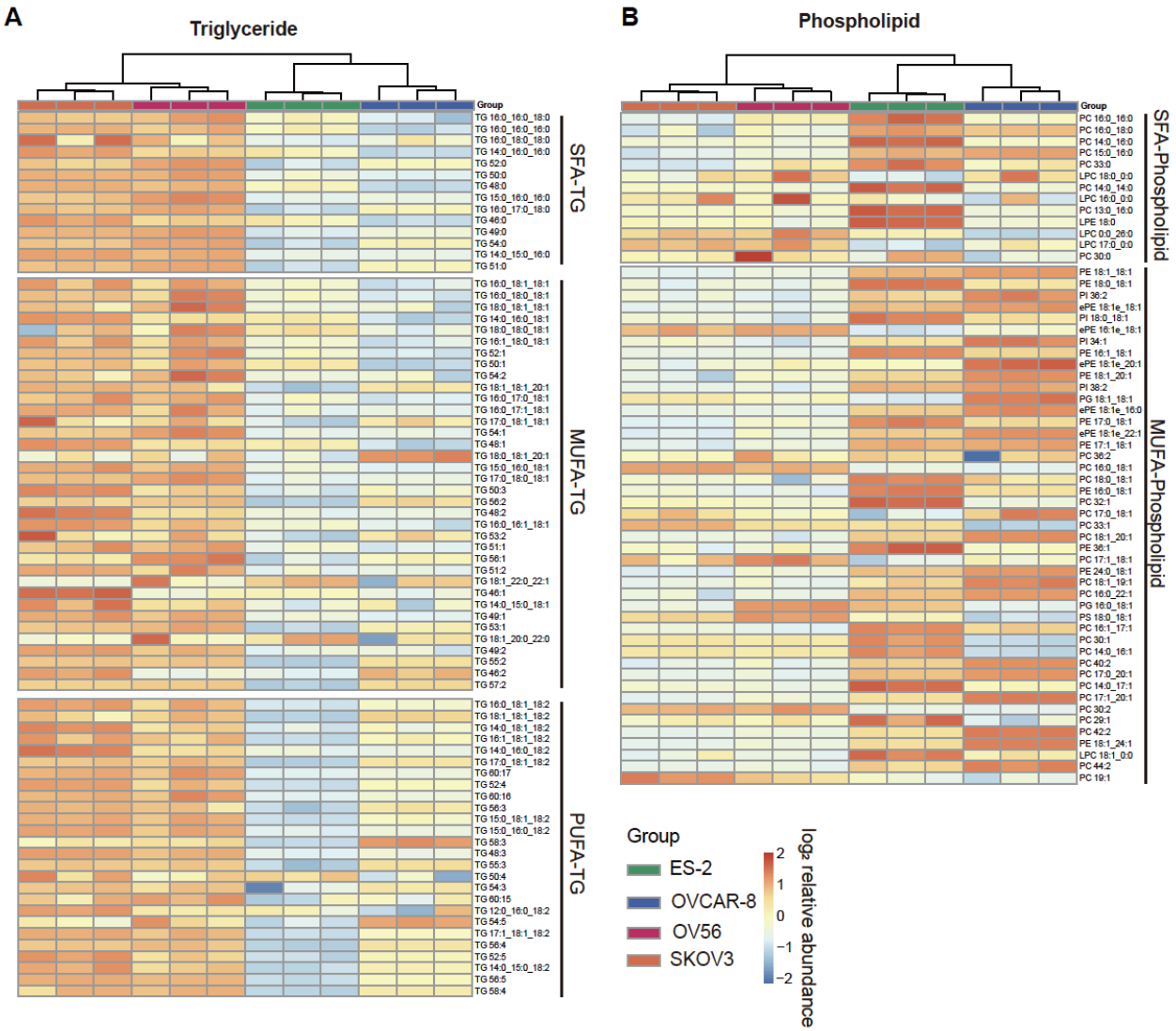

Supplementary Figure 6. Lipidomics analysis across a collection of ovarian cancer cell lines in culture (related to Figure 6).

A. Heatmap presentation of lipidomic analysis results showing the triacylglyceride (TG) distribution among ES-2, OVCAR-8, OV56, and SKOV3 ovarian cancer cells. Red, high intensity; blue, low intensity. SFA, saturated fatty acyl-; MUFA, monounsaturated fatty acyl-; PUFA, polyunsaturated fatty acyl-. n=3 for each cell line.

B. Heatmap presentation of lipidomic analysis results showing the phospholipid distribution among ES-2, OVCAR-8, OV56, and SKOV3 ovarian cancer cells. Red, high intensity; blue, low intensity. n=3 for each cell line.

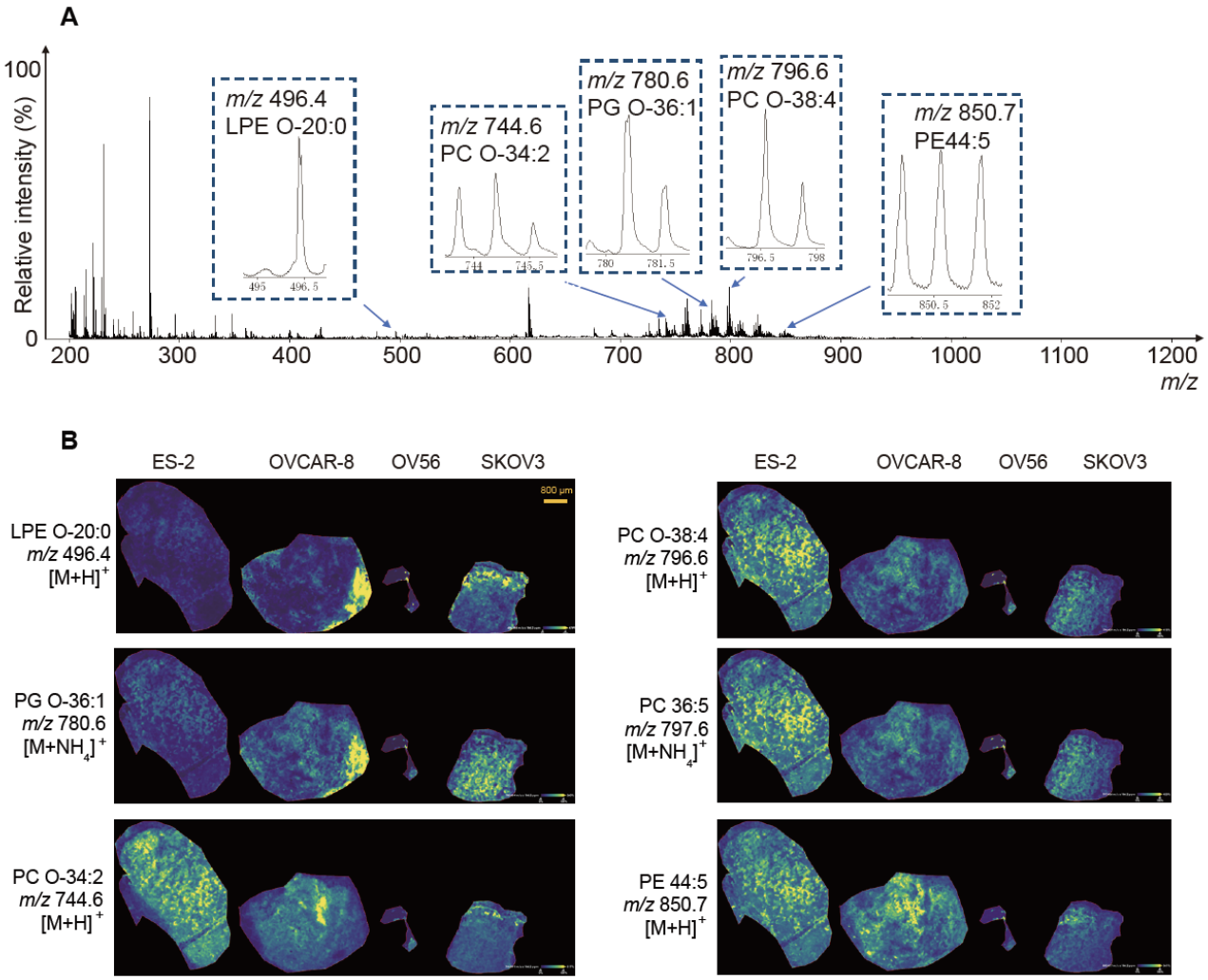

Supplementary Figure 7. MALDI-TOF mass spectrometry imaging analysis across a collection of ovarian cancer xenograft tumors (related to Figure 7).

A. Histologic examination of xenograft tumor sections using hematoxylin and eosin (H&E) staining across a collection of xenograft tumor sections including human ovarian ES-2, OVCAR-8, OV56, and SKOV3 cells. Original magnification X 200.

B. Ion features profiling of xenograft tumor sections showing representative lipid species.

C. Mass spectrometry images showing the spatial distribution of representative phospholipid on xenograft tumor sections including human ovarian ES-2, OVCAR-8, OV56, and SKOV3 cells. Yellow, high intensity; Blue, low intensity. Scale bar indicates 800 μm.